Time reversal symmetry breaking superconductivity in the honeycomb t-J model

Zheng-Cheng Gu,[1] Hong-Chen Jiang,[1,2] D. N. Sheng,[3] Hong Yao,[4] Leon Balents,[1] and Xiao-Gang Wen[5]

[1] *Kavli Institute for Theoretical Physics, University of California, Santa Barbara, CA 93106, USA*
[2] *Center for Quantum Information, IIIS, Tsinghua University, Beijing, 100084, China*
[3] *Department of Physics and Astronomy, California State University, Northridge, California 91330,USA*
[4] *Department of Physics, Stanford University, Stanford, CA 94305, USA*
[5] *Department of Physics, Massachusetts Institute of Technology, Cambridge, Massachusetts 02139, USA*

(Dated: October 7, 2011)

We report the theoretical discovery of a novel time reversal symmetry breaking superconducting state in the t-J model on the honeycomb lattice, based on a recently developed variational method - the Grassmann tensor product state approach. As a benchmark, we use exact diagonalization (ED) and density matrix renormalization (DMRG) methods to check our results on small clusters. Remarkably, we find systematical consistency for the ground state energy as well as other physical quantities, such as the staggered magnetization. At low doping, the superconductivity coexists with anti-ferromagnetic ordering.

PACS numbers:

Introduction

Since the discovery of high-temperature superconductivity in the cuprates[1], many strongly correlated models have been intensively studied. One of the simplest of these is the t-J model[2]:

$$H_{t-J} = t \sum_{\langle ij\rangle,\sigma} \tilde{c}^{\dagger}_{i,\sigma}\tilde{c}_{j,\sigma} + h.c. + J\sum_{\langle ij\rangle}\left(\boldsymbol{S}_i\cdot\boldsymbol{S}_j - \frac{1}{4}n_i n_j\right), \tag{1}$$

where $\tilde{c}^{\dagger}_{i,\sigma}$ is the electron operator defined in the no-double-occupancy subspace. This model can be derived from the strong-coupling limit of the Hubbard model. Despite its simplicity and extensive study, the nature of the ground states of Eq. (1) is still controversial.

A strong correlation view of the t-J model was advanced by Anderson, who conjectured the relevance of a Resonating Valence Bond (RVB) state[3] as a low energy state for Eq. (1) when doped. When undoped, the RVB state is a spin singlet, with no symmetry breaking, and describes a "quantum spin liquid". At low temperature the mobile carriers in the doped RVB state behave as bosons and condense, forming a state indistinguishable in terms of symmetry from a singlet BCS superconductor. A further development was the introduction of a projected mean-field wavefunction – the projection removing all components of the wavefunction with doubly occupied sites – which could be used variationally[4, 5]

Presently, this variational method remains one of the few numerical tools to study t-J like models which work directly at $T = 0$ and can treat significant system sizes. However, due to the special form of the variational wavefunction, one may be concerned about bias: very general states in the low energy subspace cannot be investigated.

Recently new numerical tools have been developed to investigate much more general low energy states in t-J like models beyond the projective method. One novel construction builds Tensor Product States (TPS's)[7–12], which can be conveniently studied and have been applied to many spin systems[8–14]. This new class of variational states do not assume any specifical ordering pattern a priori and can describe very general states as long as their entanglement entropy satisfy perimeter law. Recently, this method has been generalized to fermionic systems[15–20]. Among many different generalizations, the Grassmann Tensor Product States (GTPS's)[20] were shown to be closely related to projective states. They are able to describe a class of projective wavefunctions faithfully, including in particular the short-range RVB states.

The TPS and GTPS construction is particularly well suited to trivalent lattices, the simplest of which is the honeycomb lattice in two dimensions. Like the square lattice appropriate for the cuprates, the honeycomb lattice is bipartite and naturally supports an antiferromagnetic (AF) state at half-filling in the strong coupling (Heisenberg) limit. Similarities to cuprate physics may be expected. Moreover, several numerical studies have identified a possible quantum spin liquid state on this lattice at half-filling when additional quantum fluctuations are included in the Hubbard[6] and Heisenberg[21, 22] models. Thus the doped t-J model on the honeycomb lattice seems a promising venue to explore RVB ideas.

Here, we investigate the ground state of this system using the recently developed GTPS approach. The GTPS results are benchmarked by comparison with exact diagonalization (ED) and density matrix renormalization group (DMRG) calculations. Our results are systematically consistent with these non-variational, exact methods on small clusters. The principle result of the GTPS calculations is that the ground state at non-zero doping is a time reversal symmetry breaking $d+id$ wave superconductor. Some physical rationale for this result are given at the end of this Letter.

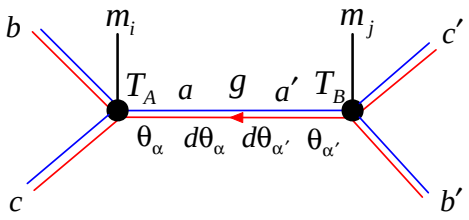

FIG. 1: Graphic representation of the GTPS on a honeycomb lattice. $\mathbf{T}_A$ and $\mathbf{T}_B$, which contain θ are defined on the sublattices A and B for each unit cell. The Grassmann metric $\mathbf{g}$ containing $\mathrm{d}\theta$ is defined on the links that connect the Grassmann tensors $\mathbf{T}_A$ and $\mathbf{T}_B$. The blue lines represent the fermion parity even indices while the red lines represent the fermion parity odd indices of the virtual states. Notice an arrow from A to B represents the ordering convention $\mathrm{d}\theta_\alpha \mathrm{d}\theta_{\alpha'}$ that we use for the Grassmann metric.

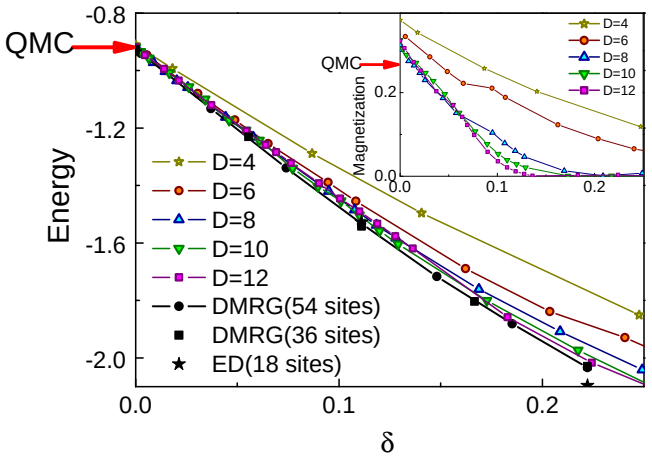

FIG. 2: Ground state energy as a function of doping. As a benchmark, we performed the ED calculation and DMRG calculations for small system size. Insert: Stagger magnetization as a function of doping.

Results

The variational ansatz: We use the standard form of GTPS as our variational wavefunction. We further assume a translationally invariant ansatz, and thus is specified by just two different Grassmann tensors $\mathbf{T}_A, \mathbf{T}_B$ on sublattice A, B of each unit cell:

$$\begin{aligned}&\Psi(\{m_i\},\{m_j\}) \qquad (2)\\ &= \mathrm{tTr}\int \prod_{\langle \mathrm{ij}\rangle} \mathbf{g}_{\mathrm{aa'}} \prod_{\mathrm{i}\in \mathrm{A}} \mathbf{T}^{\mathrm{m_i}}_{\mathrm{A;abc}} \prod_{\mathrm{j}\in \mathrm{B}} \mathbf{T}^{\mathrm{m_j}}_{\mathrm{B;a'b'c'}},\end{aligned}$$

with

$$\begin{aligned}\mathbf{T}^{m_i}_{A;abc} &= T^{m_i}_{A;abc}\theta^{P^f(a)}_\alpha \theta^{P^f(b)}_\beta \theta^{P^f(c)}_\gamma,\\ \mathbf{T}^{m_j}_{B,a'b'c'} &= T^{m_j}_{B;a'b'c'}\theta^{P^f(a')}_{\alpha'} \theta^{P^f(b')}_{\beta'} \theta^{P^f(c')}_{\gamma'},\\ \mathbf{g}_{aa'} &= \delta_{aa'}\mathrm{d}\theta^{P^f(a)}_\alpha \mathrm{d}\theta^{P^f(a')}_{\alpha'}. \qquad (3)\end{aligned}$$

We notice the symbol tTr means tensor contraction of the inner indices $\{a\}$. Here $\theta_{\alpha(\beta,\gamma)}, \mathrm{d}\theta_{\alpha(\beta,\gamma)}$ are the Grassmann numbers and dual Grassmann numbers, respectively, defined on the link $a(b,c)$, which satisfy the Grassmann algebra:

$$\begin{aligned}&\theta_\alpha\theta_\beta = -\theta_\beta\theta_\alpha, \qquad \mathrm{d}\theta_\alpha \mathrm{d}\theta_\beta = -\mathrm{d}\theta_\beta \mathrm{d}\theta_\alpha,\\ &\int \mathrm{d}\theta_\alpha\theta_\beta = \delta_{\alpha\beta} \qquad \int \mathrm{d}\theta_\alpha 1 = 0. \qquad (4)\end{aligned}$$

As shown in Fig.1, $a, b, c = 1, 2, \ldots, D$ are the virtual indices carrying a fermion parity $P^f(a) = 0, 1$. In this paper, we choose D to be even and assume there are *equal* numbers of fermion parity even/odd indices, which might be not necessary in general. Those indices with odd parity are always associated with a Grassmann number on the corresponding link and the metric $\mathbf{g}_{aa'}$ is the Grassmann generalization of the canonical delta function. The complex coefficients $T^{m_i}_{A;abc}$ and $T^{m_j}_{B;a'b'c'}$ are the variational parameters.

Notice that m_i is the physical index of the t-J model on site i, which can take three different values, $o, \uparrow$ and $\downarrow$, representing the hole, spin-up electron and spin-down electron states. We choose the hole representation in our calculations, and thus the hole state has an odd parity $P^f(o) = 1$ while the electron states have even parity $P^f(\uparrow, \downarrow) = 0$. On each site, the non-zero components of the Grassmann tensors should satisfy the parity conservation constraint:

$$P^f(m_i) + P^f(a) + P^f(b) + P^f(c) = 0 (\mathrm{mod}\, 2). \qquad (5)$$

Since the wavefunction Eq.(3) does not have a definite fermion number, we use the grand canonical ensemble, adding a chemical potential term to Eq.(1) to control the average hole concentration.

We use the imaginary time evolution method[23] to update the GTPS from a random state. Then we use the weighted Grassmann-tensor-entanglement renormalization group (wGTERG) method[20, 23] to calculate physical quantities.(See methods section for details.) The total system size ranges up to 2×27^2 sites and all calculations are performed with periodic boundary conditions. The largest virtual dimension of the GTPS considered was 12. To ensure convergence of the wTERG method, we kept D_{cut} (defined in Refs. [20, 23]) up to 130 for $D = 4, 6, 8, 10$, which gave relative errors for physical quantities of order 10^{-3}. For $D = 12$, we kept D_{cut} up to 152.

Ground state energy and staggered magnetization: At half-filling, the t-J model reduces to the Heisenberg model. In this case, we find the converged ground state energies per site are -0.5439 for $D = 10$ and -0.5441 for $D = 12$(the term $-\frac{1}{4}n_i n_j$ is subtracted

here), which is consistent with previous TPS study[12] (with virtual dimension $D = 5$ and 6, since all the components of GTPS with odd fermion parity virtual indices vanish in this case) and a recent Quantum Monte Carlo (QMC) result $E = -0.54455(20)$. Despite good agreement with the ground state energy, the staggered magnetization m obtained from our calculations is larger than the QMC result $m = 0.2681(8)$. We find $m = 0.3257$ for $D = 10$ and $m = 0.3239$ for $D = 12$, also consistent with the previous TPS study[10–12].

Nevertheless, we emphasize that the variational approach indeed obtains the correct phase. Actually, a recent study for square lattice Heisenberg model shows m can be consistent with the Quantum Monte Carlo (QMC) result if D is sufficient large[24].

Much more interesting physics arises after we dope the system.(We consider $t/J = 3$). As seen in Fig.2, the ground state energy shows a marked increase in D dependence with increasing hole doping δ. As a benchmark, we perform the ED and DMRG calculations for small periodic clusters with N sites ($N = 18$ for ED and $N = 36, 54$ for DMRG). These two methods are the only unbiased methods for frustrated systems that avoid the sign problem, but are restricted to relatively small systems. To ensure the convergence of the DMRG, we keep up to 8000 states and make the truncation errors less than 10^{-9} in our $N = 54$ calculations. Up to $D = 10$, we find a systematic convergence of the ground energy. Some data points around $\delta = 0.1$ for $D = 12$ have slightly higher energy than $D = 10$, because $D_{cut} = 152$ is still not large enough for convergence at $D = 12$.

As shown in the insert of Fig.2, the staggered magnetization m has an even larger D dependence than energy at finite doping. However, up to $D = 12$, the data appears to converge to a relatively well-defined curve indicating vanishing AF order for $\delta \gtrsim 0.1$.

Superconductivity: Next we turn to the interesting question of whether the doped antiferromagnetic Mott insulator on the honeycomb lattice supports superconductivity, and if so, what its pairing symmetry is. To answer this, we calculate the real space superconducting (SC) order parameters in the spin singlet channel $\Delta^s = \frac{1}{\sqrt{2}}(c_{i,\uparrow}c_{j,\downarrow} - c_{i,\downarrow}c_{j,\uparrow})$, where i and j are nearest neighboring sites.Because we use a chemical potential to control the hole concentration, the charge $U(1)$ symmetry can be spontaneous broken in the variational approach, which allows Δ^s to be directly measured rather than through its two-point correlation function. As shown in the main panel of Fig.3, up to $\delta = 0.15$ we find a non-zero singlet SC order parameter for the whole region. Strikingly, we find that the SC state breaks time reversal symmetry. By measuring the SC order parameters for the three inequivalent nearest-neighbor bonds, we found $\Delta^s_a/\Delta^s_b = \Delta^s_b/\Delta^s_c = \Delta^s_c/\Delta^s_a = e^{i\theta}$ with $\theta = \pm\frac{2\pi}{3}$. This pairing symmetry is usually called $d + id$ wave. To exclude the possibility that this results from trapping in a unstable local minimum, we repeated the calculations with many different random tensors, and all cases converged to the same results. Moreover, we also checked that the SC order parameter vanishes at large t/J to make sure that the existing of SC order is consequence of spontaneous symmetry breaking.(For $D = 6$, the critical value is around 15 at $\delta \sim 0.3$)

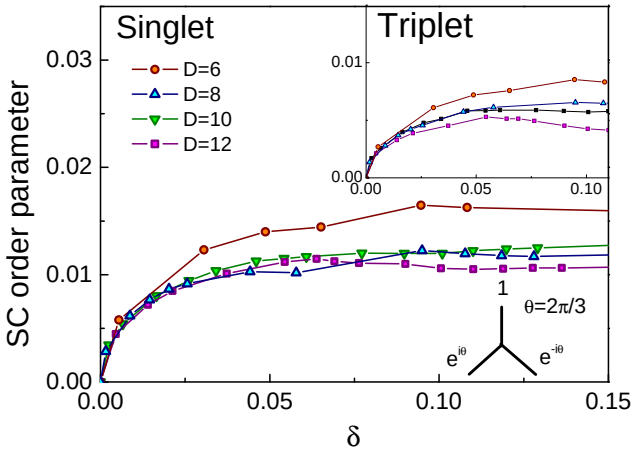

FIG. 3: SC order parameters as a function of doping.

The existence of SC order is observed in our numerical study up to $\delta = 0.4$. However, a much larger inner dimension D is required for the convergence of ground state energy at larger hole concentration, which is beyond the scope of this paper.(The GTPS variational ansatz we use in this paper is designed to help us understand the nature of Mott physics; at large doping, the Mott physics becomes less important and can be studied much better by other methods.)

Coexisting phases at low doping: Interestingly, we find the SC and AF order coexisting in the regime $0 < \delta < 0.1$. A physical consequence of the microscopic coexistance is that triplet pairing is induced. The insert of Fig.3 shows the amplitude of the triplet order parameter as a function of doping. Since the triplet pairing order parameter has three independent components $\vec{\Delta}_t = \frac{1}{\sqrt{2}}c_{i,\alpha}(i\sigma^y\vec{\sigma})_{\alpha\beta}c_{j,\beta} = \mathbf{d}e^{i\phi}$(Here $i \in A$, $j \in B$ and ϕ is the phase of SC order parameter.), we can define the amplitude of triplet order parameter as $\Delta_t = \sqrt{\vec{\Delta}^*_t \cdot \vec{\Delta}_t}$.

The phase shift of $2\pi/3$ on the three inequivalent bonds is also observed for all the triplet components. We further check the internal spin direction of the triplet $\boldsymbol{d}$ vector and find it is always anti-parallel to the Neel vector($\boldsymbol{S}_{\rm Neel} = \langle \boldsymbol{S}_i \rangle - \langle \boldsymbol{S}_j \rangle$). At larger doping $\delta > 0.1$, the triplet order parameter has a very strong D dependence, so at present we are unable to determine whether it ultimately vanishes or remains non-zero in the $D \to \infty$ limit. We leave this issue for future work. By fully using

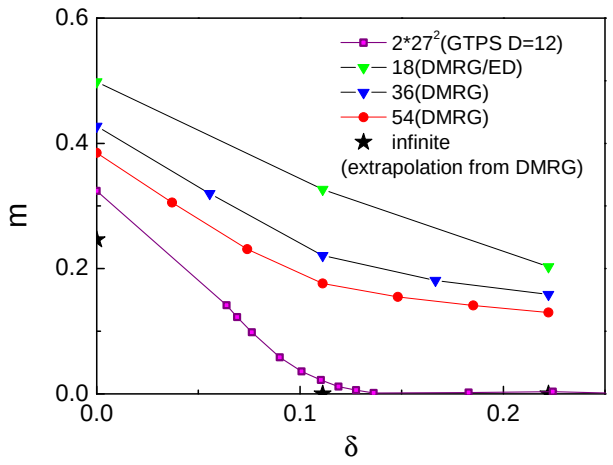

FIG. 4: The comparison of DMRG/ED and GTPS calculations for stagger magnetization m.

all symmetry quantum numbers and other techniques like high performance simulation on GPUs, we can in principle handle D up to $20-30$.

Discussion

The calculations in this paper by construction ignore any possible phases breaking translational symmetry. Natural candidates are spiral or striped antiferromagnetic phases, as have been heavily discussed for the square lattice. A weak coupling perspective suggests this may be unlikely.

In the weak-coupling limit of Hubbard model on honeycomb lattice, the system is a semimetal with two Dirac cones. With a non-zero Hubbard U, commensurate AF fluctuations at zero momentum manifest in the inter-band susceptibility, becoming stronger and stronger with increasing U. At sufficiently large U commensurate AF order develops (recent numerics find a narrow region of intermediate spin liquid phase[6]). At small but finite doping, the Dirac cones become pockets. In this case, the total intra-band spin susceptibility shows a constant behavior for small $q(q < 2k_f)$[25] while the total inter-band spin susceptibility still peaks at zero momentum. Thus, we argue the commensurate AF fluctuations at zero momentum still dominate for sufficient small hole concentration.

Our DMRG and ED calculations also support this argument. Up to 54 sites, we do not find any evidence of incommensurate spin-spin correlation. Fig.4 shows the comparison of DMRG calculations and GTPS calculations for staggered magnetization m on small systems. We find the GTPS results are comparable with extrapolations of m for infinite size systems (the GTPS results for m are somewhat larger close to half-filling due to insufficient tensor dimension D). This agreement also implies our variational wavefunction is very close to the true ground state.

A more general concern is whether the GTPS tends to overestimate SC order at large doping, due to its non-conservation of charge(note that the projected wavefunction approach has a rather strong tendency to produce superconducting states). The observed SC order parameter is "small" in terms of the natural upper limit $\langle cc\rangle \lesssim 0.1\delta \ll \delta$. Nevertheless, our results are consistent with other approaches: (a) in the mean field theory for the honeycomb $t-J$ model, only the $d+id$ pairing channel gains energy[26], and (b) in the weak coupling limit of Hubbard model, very recent renormalization group studies also find $d+id$ superconductivity around quarter filling[27–29].

In conclusion, we report the theoretical discovery of a $d+id$ wave superconducting state in t-J model on a honeycomb lattice, based on a recently developed variational method - the GTPS approach. At low doping, AF ordering coexists with the SC ordering. In the coexistance regime, a spin triplet pairing with the same phase shift is induced and its triplet $\mathbf{d}$ vector is anti-parallel with the Neel vector. It would be interesting to search for this physics in experiment. The recently discovered spin 1/2 honeycomb lattice antiferromagnet $InV_{1/3}Cu_{2/3}O_3$[30] would be an appealing candidate if it could be doped.

Methods

The imaginary time evolution algorithm of GTPS: In this paper, we use the (simplified) imaginary time evolution method[23] to update the GTPS variational wave function. In the hole representation, we can decompose the $\tilde{c}^\dagger_{i,\sigma}$ as $\tilde{c}_{i,\sigma} = h^\dagger_i b_{i;\sigma}$. Here the holon h_i is a fermion while the spinon $b_{i;\sigma}$ is a boson. The no-double-occupancy constraint reads:

$$\sum_\sigma b^\dagger_{i;\sigma} b_{i;\sigma} + h^\dagger_i h_i = 1 \tag{6}$$

Under this representation, we can rewrite the $t-J$ model as:

$$H_{t-J} = -t\sum_{\langle ij\rangle,\sigma} h^\dagger_j h_i b^\dagger_{i;\sigma} b_{j;\sigma} + h.c. + J\sum_{\langle ij\rangle}\left(\boldsymbol{S}_i\boldsymbol{S}_j - \frac{1}{4}n^b_i n^b_j\right), \tag{7}$$

where

$$\boldsymbol{S}_i = \sum_{\sigma\sigma'} b^\dagger_{i;\sigma}\tau_{\sigma\sigma'} b_{i;\sigma'}; \quad n^b_i = \sum_\sigma b^\dagger_{i;\sigma} b_{i;\sigma} \tag{8}$$

Due to the no-double-occupancy constraint Eq. (6), the spin up/down states $|\uparrow(\downarrow)_i\rangle = b^\dagger_{i;\uparrow(\downarrow)}|0\rangle$ and the hole state $|o\rangle = h^\dagger_i|0\rangle$ form a complete basis for each site. The

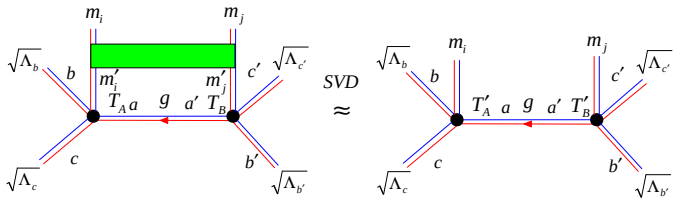

FIG. 5: A schematic plot for the imaginary time evolution algorithm.

closure condition reads:

$$|\uparrow_i\rangle\langle\uparrow_i| + |\downarrow_i\rangle\langle\downarrow_i| + |o_i\rangle\langle o_i| = 1 \tag{9}$$

As already has been discussed in Ref.[23], we need to use the fermion coherent state representation to perform the imaginary time evolution algorithm for GTPS. Let us introduce the fermion coherent state of holon $|\eta_i\rangle = |0\rangle - \eta_i h_i^\dagger|0\rangle$.($\eta_i$ is a Grassmann variable here.) In this new basis, the closure relation Eq. (10) becomes:

$$|\uparrow_i\rangle\langle\uparrow_i| + |\downarrow_i\rangle\langle\downarrow_i| + \int \mathrm{d}\bar{\eta}_i \mathrm{d}\eta_i |\eta_i\rangle\langle\bar{\eta}_i| = 1 \tag{10}$$

The variational ground state can be determined through imaginary time evolution:

$$|\Psi_G\rangle = e^{-\tau H_{t-J}}|\Psi_0\rangle, \quad \tau \to \infty \tag{11}$$

For sufficient thin time slice $\delta\tau$, we can decompose $e^{-\delta\tau H_{t-J}}$ as:

$$e^{-\delta\tau H_{t-J}} \sim e^{-\delta\tau H^x_{t-J}} e^{-\delta\tau H^y_{t-J}} e^{-\delta\tau H^z_{t-J}} \tag{12}$$

Here x, y, z represent three different directions of the honeycomb lattice and each $H^{x(y,z)}_{t-J}$ term contains a summation of non-overlapped two body Hamiltonian $H^{x(y,z)}_{t-J} = \sum_{\langle ij\rangle} h^{x(y,z)}_{ij}$. Thus, for sufficient thin time slice, we can apply the evolution operator along $x(y,z)$ direction separately.

In the fermion coherent state representation, the two body evolution operator along x direction $e^{-\delta h^x_{ij}}$ can be expressed as a Grassmann valued matrix acting on the two sites Hilbert space:

$$\begin{aligned}&\langle \mathfrak{m}_i \mathfrak{m}_j | e^{-\delta\tau h^x_{ij}} | \mathfrak{m}'_i \mathfrak{m}'_j \rangle \\ =&E^{m_i m_j}_{m'_i m'_j} (\eta_j)^{P^f(m_j)} (\eta_i)^{P^f(m_i)} (\bar{\eta}'_i)^{P^f(m'_i)} (\bar{\eta}'_j)^{P^f(m'_j)}\end{aligned} \tag{13}$$

Here $\mathfrak{m}_i$ is the fermion coherent states indices valued as $\uparrow, \downarrow$ or η while m_i is the usual Fock state indices valued as $\uparrow, \downarrow$ or o. We notice the spin states remain the same in both representations.

By applying the method developed in Ref.[23], we can successfully update the (complex) variational parameters $T^{m_i}_{A;abc}$ and $T^{m_j}_{B;a'b'c'}$ as:

$$\begin{aligned} T'^{m_i}_{A;abc} &= (-)^{P^f(m_i)P^f(a)} \frac{\sqrt{\Lambda'_a}}{\sqrt{\Lambda^y_b}\sqrt{\Lambda^z_c}} U_{bcm_i;a} \\ T'^{m_j}_{B;a'b'c'} &= (-)^{P^f(m_j)P^f(a')} \frac{\sqrt{\Lambda'_{a'}}}{\sqrt{\Lambda^y_{b'}}\sqrt{\Lambda^z_{c'}}} V_{b'c'm_j;a'}, \end{aligned} \tag{14}$$

where U and V are determined by the singular value decomposition(SVD) of the following matrix M:

$$\begin{aligned} \mathrm{M}_{bcm_i;b'c'm_j} = &\sum_{am'_i m'_j} \sqrt{\Lambda^y_b}\sqrt{\Lambda^z_c}\sqrt{\Lambda^y_{b'}}\sqrt{\Lambda^z_{c'}} \\ &\times (-)^{\left[P^f(m'_i)+P^f(m'_j)\right]P^f(a)} (-)^{P^f(m'_j)\left[P^f(m'_i)+P^f(b)+P^f(c)\right]} \\ &\times (-)^{m_j\left[P^f(m_i)+P^f(b)+P^f(c)\right]} E^{m_i m_j}_{m'_i m'_j} T^{m'_i}_{A;abc} T^{m'_j}_{B;ab'c'} \end{aligned} \tag{15}$$

We keep the largest Dth singular values:

$$\mathrm{M}_{bcm_i;b'c'm_j} \simeq \sum_{a=1}^{D} U_{bcm_i;a} \Lambda'_a V_{b'c'm_j;a} \tag{16}$$

Similar as in the usual TPS case[10], the environment weight vectors $\Lambda^{x(y,z)}$ can be initialized as 1 and then updated during the time evolution. For example, Λ^x is updated as Λ' in the above evolution scheme.

The GTERG/wGTERG algorithm: After determining the variational ground state of GTPS by performing the imaginary time evolution, we can compute the physical quantities by using the GTERG/wGTERG method developed in Ref[20, 23]. This method can be regarded as the Grassmann variable generalization of the usual TERG/wTERG method[9, 23], where a coarse graining procedure is designed to calculate the physical quantities of TPS efficiently. In Fig.7, we plot the variational ground state energy($D = 10$) as a function of doping with different D_{cut}(Number of eigenvalues kept in the wGTERG algorithm). We find the relative error is of order 10^{-3}.

Acknowledgment

The authors would like to thank F. Verstraete, J. I. Cirac, M. P. A. Fisher, F. C. Zhang, P. A. Lee, Z. Y. Weng, L. Fu, K. Sun, C. Wu, F. Yang and Y. Zhou for valuable discussions. Z.C.G. is supported by NSF Grant No. PHY05-51164; D.N.S is supported by DMR-0906816; L.B. is supported by NSF grant DMR-0804564 and a Packard Fellowship; H.Y. was partly supported by DOE grant DE-AC02-05CH11231; X.G.W. is supported by NSF Grant No. DMR-1005541 and NSFC 11074140.

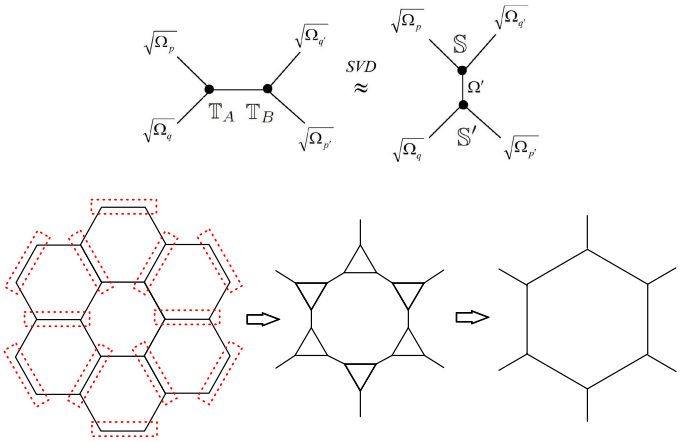

FIG. 6: A schematic plot for the renormalization algorithm on honeycomb lattice. Similar as the simplified imaginary time evolution algorithm, we use a weighting vector $\sqrt{\Omega}$ to mimic the environment effect. As has been discussed in Ref.[23], the initial value of Ω can be determined by Λ on the corresponding link and will be updated during the RG scheme.

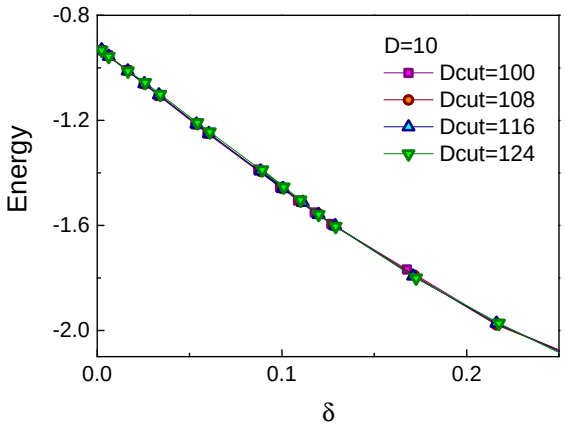

FIG. 7: Variational ground state energy($D = 10$) as a function of doping with different D_{cut}(Number of eigenvalues kept in the wGTERG algorithm). It is shown all the data points almost collapse on the same curve. We find the relative error is of order 10^{-3}.

[1] J. G. Bednorz and K. A. Mueller, Possible High T_c Superconductivity in the Ba-La-Cu-O System, Z. Phys. B **64**, 189 (1986).

[2] F. C. Zhang and T. M. Rice, Effective Hamiltonian for the superconducting Cu oxides, Phys. Rev. B **37**, 3759 (1988).

[3] P. W. Anderson The resonating valence bond state in La_2CuO_4 and superconductivity, Science **235**, 1196 (1987).

[4] C. Gros Superconductivity in correlated wave functions, Phys. Rev. B **38**, 931 (1988).

[5] For a review, see P. A. Lee, N. Nagaosa and X. G. Wen, Doping a Mott insulator: Physics of high-temperature superconductivity, Phys. Mod. Phys. **78**, 17 (2006).

[6] Z. Y. Meng, T. C. Lang, S. Wessel, F. F. Assaad and A. Muramatsu, Quantum spin liquid emerging in two-dimensional correlated Dirac fermions, Nature **464**, 847 (2010).

[7] F. Verstraete and J. I. Cirac, Renormalization algorithms for Quantum-Many Body Systems in two and higher dimensions, (2004), arXiv:cond-mat/0407066.

[8] J. Jordan, R. Orus, G. Vidal, F. Verstraete, and J. I. Cirac, Classical Simulation of Infinite-Size Quantum Lattice Systems in Two Spatial Dimensions, Physical Review Letters **101**, 250602 (2008).

[9] Z.-C. Gu, M. Levin, and X.-G. Wen, Tensor-entanglement renormalization group approach as a unified method for symmetry breaking and topological phase transitions, Phys. Rev. B **78**, 205116 (2008).

[10] H. C. Jiang, Z. Y. Weng, and T. Xiang, Accurate Determination of Tensor Network State of Quantum Lattice Models in Two Dimensions, Phys. Rev. Lett. **101**, 090603 (2008);

[11] Z. Y. Xie, H. C. Jiang, Q. N. Chen, Z. Y. Weng, and T. Xiang, Second Renormalization of Tensor-Network States, Phys. Rev. Lett. **103**, 160601 (2009);

[12] H. H. Zhao, Z. Y. Xie, Q. N. Chen, Z. C. Wei, J. W. Cai,and T. Xiang, Renormalization of tensor-network states, Phys. Rev. B **81**, 174411 (2010).

[13] B. Bauer, G. Vidal, and M. Troyer, Assessing the accuracy of projected entangled-pair states on infinite lattices, J.Stat.Mech. (2009). p09006.

[14] V. Murg, F. Verstraete, and J. I. Cirac, Exploring frustrated spin systems using projected entangled pair states, Phys. Rev. B **79**, 195119 (2009).

[15] C. V. Kraus, N. Schuch, F. Verstraete, and J. I. Cirac Fermionic Projected Entangled Pair States, Phys. Rev. A **81**, 052338 (2010).

[16] P. Corboz, R. Orus, B. Bauer,and G. Vidal, Simulation of strongly correlated fermions in two spatial dimensions with fermionic Projected Entangled-Pair States, Phys. Rev. B **81**, 165104 (2010).

[17] T. Barthel, C. Pineda, and J. Eisert, Contraction of fermionic operator circuits and the simulation of strongly correlated fermions, Phys. Rev. A **80**, 042333 (2009).

[18] Q. Q. Shi, S. H. Li, J. H. Zhao, and H. Q. Zhou, Graded Projected Entangled-Pair State Representations and An Algorithm for Translationally Invariant Strongly Correlated Electronic Systems on Infinite-Size Lattices in Two Spatial Dimensions, (2009), arXiv:cond-mat/0907.5520.

[19] Iztok Pizorn, and Frank Verstraete, Fermionic Implementation of Projected Entangled Pair States Algorithm, Phys. Rev. B **81**, 245110 (2010).

[20] Z.-C. Gu, F. Verstraete, and X.-G. Wen, Grassmann tensor network states and its renormalization for strongly correlated fermionic and bosonic states, (2010), arXiv:cond-mat/1004.2563.

[21] J. B. Fouet, P. Sindzingre, and C. Lhuillier, An investigation of the quantum J_1-J_2-J_3 model on the honeycomb lattice, Eur. Phys. J. B **20**, 241 (2001).

[22] B. K. Clark, D. A. Abanin, and S. L. Sondhi, Nature of the spin liquid state of the Hubbard model on honeycomb lattice, Phys. Rev. Lett. **107**, 087204 (2011);

[23] Z.-C. Gu, Efficient simulation of Grassmann Tensor

Product States, (2011),arXiv:cond-mat/1109.4470.
[24] Ling Wang, Iztok Pizorn, and Frank Verstraete, Monte Carlo simulation with Tensor Network States, Phys. Rev. B **83**, 134421 (2011).
[25] E. H. Hwang, and S. Das Sarma, Dielectric function, screening, and plasmons in two-dimensional graphene, Phys. Rev. B **75**, 205418 (2007).
[26] A. M. Black-Schaffer, and S. Doniach, Resonating valence bonds and mean-field d-wave superconductivity in graphite, Phys. Rev. B **75**, 134512 (2007).
[27] R. Nandkishore, L. Levitov, and A. Chubukov, Chiral superconductivity from repulsive interactions in doped graphene, (2011),arXiv:cond-mat/1109.3884.
[28] W.-S. Wang, Y.-Y. Xiang, Q.-H. Wang, F. Wang, F. Yang, and D. H. Lee, Functional renormalization group and variational Monte Carlo studies of the electronic instabilities in graphene near 1/4 doping, (2011),arXiv:cond-mat/1109.3884.
[29] M. Kiesel, C. Platt, W. Kanke, D. A. Abanin, and R. Thomale, Competing many-body instabilities and unconventional superconductivity in graphene, (2011),arXiv:cond-mat/1109.2953.
[30] A. Möller, U. Löw, T. Taetz, M. Kriener, G. André, F. Damay, M. Braden, and J. A. Mydosh, Structural domain and finite-size effects of the antiferromagnetic S=1/2 honeycomb lattice in $InCu_{2/3}V_{1/3}O_3$, Phys. Rev. B **78**, 024420 (2008).